Available online at www.sciencedirect.com

ScienceDirect

Procedia Structural Integrity 79 (2026) 9–16

Structural Integrity Procedia

www.elsevier.com/locate/procedia

28th International Conference on Fracture and Structural Integrity - 3rd Mediterranean Conference on Fracture and Structural Integrity

Development and Mechanical Characterization of a Novel Ni-Ti Based Damping Seismic Device

Girolamo Costanza[a], Alessandro Molinari[a], Ilaria Porroni[a,*], Maria Elisa Tata[a]

[a]*Industrial Engineering Department, University of Rome "Tor Vergata", 00133 Rome, Italy;*

Abstract

Traditional seismic devices suffer from residual deformation issues that compromise structural resilience and require extensive post-earthquake repairs. An innovative seismic self-centering device based on Ni-Ti shape memory elements for enhanced structural performance and damping is presented in this work. The investigation encompasses both L-shaped sheet and helical spring configurations tested under quasi-static conditions, with individual component characterization across two temperature conditions (25°C and 100°C), followed by comprehensive evaluation of assembly configurations including Ni-Ti sheets, steel baseline comparison, and combined Ni-Ti sheet-spring systems.

Experimental results demonstrate distinct performance trade-offs among SMA configurations. Combined Ni-Ti sheet-spring assemblies optimize self-centering capability (99.5% recovery) with highest force capacity (224.5N) but reduced energy dissipation ($8.1 \times 10^4 J/m^3$), while individual L-shaped Ni-Ti sheet configurations provide balanced performance across all metrics, showing promising characteristics in terms of load, displacement and energy dissipation.

Temperature analysis revealed substantial force enhancement of +121% from 25°C to 100°C at 2.5mm displacement, establishing thermal control as a design parameter. At 25°C, L-shaped configurations achieve forces of 40.9-206.8N with energy dissipation of $8.1 \times 10^3 - 1.89 \times 10^5 J/m^3$, while elevated temperature testing demonstrates enhanced force capacity up to 405N with increased energy dissipation up to $2.82 \times 10^5 J/m^3$. The experimental results demonstrate that the proposed SMA sheet configurations exhibit reliable energy dissipation characteristics, maintaining consistent self-centering capabilities across the tested temperature and load range. These findings establish experimental foundation for future dynamic validation studies and contribute to the advancement of SMA-based damping systems for structural seismic protection.

© 2025 The Authors. Published by ELSEVIER B.V.
This is an open access article under the CC BY-NC-ND license (https://creativecommons.org/licenses/by-nc-nd/4.0)
Peer-review under responsibility of IGF28 - MedFract3 organizers

Keywords: Shape memory alloys; seismic devices; self-centering; superelasticity; energy dissipation; Ni-Ti.

1. Introduction

Traditional seismic design approaches have primarily focused on preventing structural collapse, often neglecting post-earthquake recovery, as highlighted by Costanza et al. (2024). Structures with conventional damping systems

* Corresponding author.
E-mail address: ilaria.porroni@alumni.uniroma2.eu

2452-3216 © 2025 The Authors. Published by ELSEVIER B.V.
This is an open access article under the CC BY-NC-ND license (https://creativecommons.org/licenses/by-nc-nd/4.0)
Peer-review under responsibility of IGF28 - MedFract3 organizers
10.1016/j.prostr.2025.12.303

frequently exhibit substantial residual deformations following seismic events, necessitating extensive repairs and prolonged downtime. To address these issues, the concept of seismic resilience has received considerable attention, extending beyond collapse prevention to encompass operational continuity and swift recovery Mashal and Palermo (2019).

Shape memory alloys (SMA) have emerged as promising materials through their unique superelastic properties. Stress-induced phase transformation between austenite and martensite enables recoverable strains up to 8%, as reported by Costanza et al. (2024), manifesting as flag-shaped hysteretic loops that provide simultaneous energy dissipation and self-centering capabilities with minimal residual deformation Acar (2015).

Recent research has demonstrated SMA effectiveness in various seismic applications. Tensile-based systems have shown promising results in bracing applications, as demonstrated by DesRoches et al. (2004) and Miller et al. (2012), while innovative damping configurations including U-shaped (Wang and Zhu (2018)) and ring-based (Gao et al. (2016)) designs have exhibited excellent self-centering performance. Furthermore, dynamic testing has validated SMA braces efficacy in frame systems (Qiu and Zhu (2017)) and enhanced post-tensioned connections (Chowdhury et al. (2019)).

Despite these advances, current implementations predominantly focus on tensile-based configurations. Wang et al. (2020) established SMA angles reliability under cyclic loading. However, systematic investigation of bending configurations, particularly L-shaped arrangements, remains limited despite potential advantages in installation flexibility and force distribution characteristics.

The present investigation addresses this gap through comprehensive characterization of a novel L-shaped Ni-Ti seismic device, encompassing component behavior under varying temperatures, assembly configurations, and comparison with stainless steel baseline systems. Temperature effects require detailed quantification for bending-based configurations, as recently investigated by Bizzarri et al. (2025).

The primary objectives of this study include: (1) development of an innovative L-shaped Ni-Ti damping device suitable for seismic applications; (2) comprehensive mechanical characterization under quasi-static conditions across two different temperature regimes; (3) systematic evaluation of configuration trade-offs between individual sheets, combined sheet-spring assemblies, and steel baseline comparisons; and (4) quantification of temperature effects on device performance to establish thermal control as a design parameter. This static characterization provides the essential foundation for subsequent dynamic validation studies and contributes to advancing SMA-based damping systems for structural seismic protection.

2. Materials and Methods

2.1. Material Specifications

Commercial Ni-Ti alloy sheets optimized for superelastic applications were employed in this investigation, with original dimensions of $100mm \times 20mm \times 0.5mm$. The manufacturer specifications indicate characteristic transformation temperatures with martensite phase present below -10°C and an austenite finish temperature (A_f) of 5°C, ensuring superelastic behavior at room temperature conditions. Following initial characterization, the sheets were machined to final dimensions of $80mm \times 20mm \times 0.5mm$ to achieve optimal geometric parameters for the L-shaped configuration. Following dimensional preparation, controlled drilling operations created connection holes with $4mm$ diameter to accommodate mechanical fasteners while maintaining structural integrity of the SMA material.

For helical spring components, commercial Ni-Ti wire with $0.8mm$ diameter was utilized to fabricate coil springs with $6mm$ coil diameter, comprising 19 turns with a free length of $20mm$. The wire material exhibited identical transformation characteristics to the sheet material, enabling consistent superelastic response across all SMA components. Figure 1 shows the initial Ni-Ti sheet material and fabricated helical spring components.

2.2. Shape Setting and Heat Treatment

All SMA components underwent systematic shape setting procedures to establish the desired geometric configuration and optimize superelastic properties. The heat treatment protocol involved maintaining specimens at 500°C for 30 minutes in an electric furnace, followed by rapid quenching in water at room temperature. This procedure ensures the

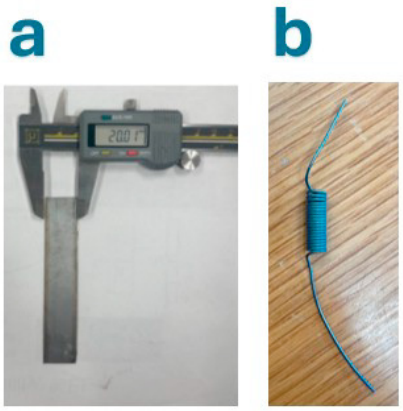


Fig. 1. Ni-Ti material components: (a) commercial sheet material and (b) fabricated helical spring from Ni-Ti wire

SMA material memorizes the imposed configuration in the austenitic phase: L-shaped geometry for sheet components and helical coil geometry for spring elements, while maintaining optimal superelastic response characteristics. Figure 2 illustrates the shape setting process and resulting L-shaped geometry after heat treatment.

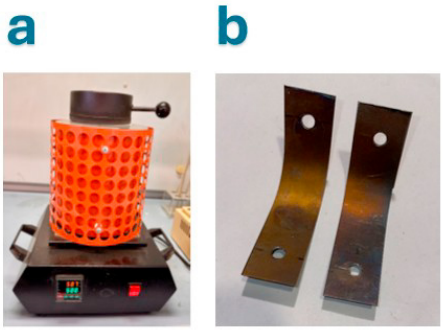


Fig. 2. Shape setting: (a) electric furnace setup and (b) L-shaped Ni-Ti sheet after heat treatment and water quenching

2.3. Device Fabrication and Assembly

The complete device fabrication process required systematic integration of multiple components to achieve a functional seismic damping prototype. Wooden support structures formed the foundation of the assembly system, providing stable mounting points and ensuring consistent boundary conditions across all testing configurations. The support elements were precision-machined from hardwood to achieve the required dimensional accuracy and structural stability.

Upper and lower support blocks were designed with integrated mounting features to accommodate the L-shaped SMA elements and enable secure attachment to the testing apparatus. The wooden components incorporated precision-drilled holes and threaded inserts to ensure reliable mechanical connections throughout the experimental program. Stainless steel threaded rods provided the primary load transfer mechanism between upper and lower supports, enabling direct force transmission through the device assembly.

The complete assembly process integrated all components through a systematic procedure designed to ensure proper alignment and consistent boundary conditions. L-shaped sheets were positioned between upper and lower support blocks using precision alignment fixtures. Mechanical fasteners secured the SMA elements while maintaining the ability to apply controlled displacements during testing. For combined configurations, helical springs were installed in

parallel with the sheet elements to provide additional elastic restoring forces. Figure 3 illustrates the complete device assembly and wooden support structure.

2.4. Experimental Approach and Device Configurations

The experimental investigation followed a systematic two-phase approach to enable comprehensive device characterization. The initial phase involved individual component testing to establish baseline mechanical properties of L-shaped Ni-Ti sheets and helical springs under controlled loading conditions. This preliminary characterization provided essential material property data and validated superelastic behavior prior to system-level assembly.

Following individual component validation, three primary seismic device configurations were assembled and systematically investigated to evaluate performance trade-offs and identify optimal design parameters. The first configuration employed dual L-shaped Ni-Ti sheets in parallel arrangement, providing baseline SMA device performance assessment under bending-dominated loading conditions. The second configuration incorporated the same dual L-shaped sheets combined with two helical Ni-Ti springs in parallel to enhance self-centering capabilities through increased elastic restoring forces. The third configuration utilized L-shaped steel sheets with identical geometric specifications, serving as a conventional material baseline for direct comparison and validation of SMA advantages.

Assembly systems employed precision-machined wooden support structures with stainless steel connection elements to ensure consistent boundary conditions across all testing configurations. Mechanical fastening systems enabled configuration variations and component replacement throughout the experimental program. Figure 3 presents the three primary device configurations investigated in this study.

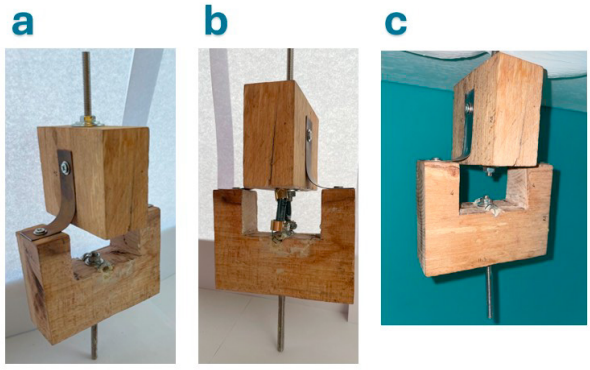


Fig. 3. Device configurations: (a) dual L-shaped Ni-Ti sheets in parallel, (b) combined sheet-spring assembly, and (c) stainless steel baseline configuration

2.5. Experimental Testing Protocols

The experimental program followed the systematic two-phase approach established in the device configuration strategy. Initial testing focused on individual component characterization to establish baseline mechanical properties and validate superelastic behavior. Individual L-shaped sheets and helical springs were tested separately using displacement-controlled loading at $20mm/min$ crosshead speed to ensure quasi-static conditions and minimize rate-dependent effects.

Following individual component validation, assembly-level testing investigated the three device configurations under identical testing protocols. For assembly testing, machine crosshead speed was set at $5mm/min$ to enable accurate force measurement during coordinated bending of multiple elements.

Mechanical characterization employed an MTS universal testing system equipped with a $50kN$ load cell and integrated thermostatic chamber for temperature-controlled testing. Testing protocols encompassed two primary temperature conditions: room temperature (25°C) and elevated temperature (100°C) to quantify thermal effects on SMA performance.

Displacement-controlled testing investigated three displacement levels: ±1.25*mm*, ±2.5*mm*, and ±5*mm* to evaluate displacement-dependent superelastic activation and energy dissipation characteristics. Cyclic loading protocols included both tension-compression loops and reverse loading sequences to assess material stability and identify potential training effects.

Data post-processing employed numerical integration techniques to quantify energy dissipation through hysteretic loop area calculation, while SEA calculations enabled configuration comparison independent of geometric scaling effects.

2.6. Performance Metrics and Calculation Methods

Comprehensive performance evaluation required systematic quantification of key seismic device characteristics through standardized calculation methodologies. Figure 4 presents a typical force-displacement hysteretic loop obtained experimentally from cyclic testing. This section illustrates the determination of all performance metrics from experimental data.

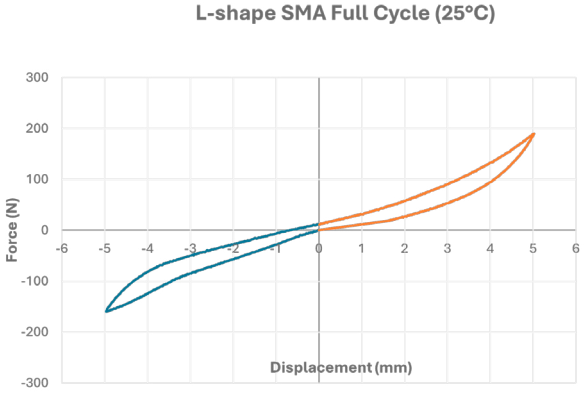


Fig. 4. Representative force-displacement hysteretic loop (L-shaped Ni-Ti assembly, 5mm displacement, 25°C)

Energy dissipation capacity was determined through numerical integration of hysteretic loops using the trapezoidal rule method. The energy dissipated per cycle corresponds to the area enclosed by the force-displacement hysteretic loop, calculated as:

$$E_{diss} = \oint F\,dx \approx \sum_{i=1}^{n} \frac{F_i + F_{i+1}}{2}(x_{i+1} - x_i) \tag{1}$$

where F represents the applied force and x the corresponding displacement. This discrete approximation enables accurate energy quantification from experimental force-displacement data pairs.

Specific abssorbed energy (SEA) provided configuration-independent performance comparison by normalizing total energy dissipation to active material volume. For individual L-shaped sheet configurations, the active volume was calculated as $V_{sheet} = 2 \times s \times b \times l$, where s, b, and l represent sheet thickness, width, and length respectively. Combined sheet-spring assemblies required summation of sheet and spring volumes:

$$V_{total} = V_{sheets} + V_{springs} = 2 \times s \times b \times l + 2 \times \pi r_{wire}^2 \times L_{wire} \tag{2}$$

where r_{wire} and L_{wire} denote wire radius and total wire length in the helical spring configuration.

Peak force capacity was identified as the maximum absolute force magnitude throughout the loading cycle, representing the device's maximum load-bearing capability. Stiffness characterization employed linear regression analysis of the initial elastic loading region to determine the force-displacement slope, providing quantitative assessment of structural rigidity.

Self-centering capability was quantified through residual displacement measurement and recovery ratio calculation. The recovery ratio represents the percentage of total displacement recovered upon complete load removal, calculated as:

$$Recovery\ Ratio = \frac{d_{max} - d_{residual}}{d_{max}} \times 100\% \tag{3}$$

where d_{max} represents maximum applied displacement and $d_{residual}$ denotes permanent deformation after unloading. This metric provides direct assessment of self-centering effectiveness.

Temperature-dependent performance analysis required systematic comparison of identical displacement protocols across thermal conditions, ensuring fair assessment of thermal effects on superelastic behavior and energy dissipation characteristics. All comparative analyses maintained consistent testing parameters (displacement amplitude, loading rate, boundary conditions) to isolate temperature effects from other experimental variables.

3. Results and Discussion

3.1. Individual Component Characterization

Individual component testing established baseline mechanical properties prior to system-level assembly. L-shaped Ni-Ti sheets demonstrated characteristic superelastic behavior with individual elements achieving peak forces of 16N at 15mm maximum displacement. Individual sheet testing confirmed flag-shaped hysteretic loops with stress-induced martensitic transformation, validating superelastic activation at room temperature conditions.

Helical spring characterization revealed pronounced temperature-dependent mechanical properties. Room temperature testing demonstrated predominantly elastic response with spring stiffness of 101.4 − 115.2N/m and peak forces limited to 3.5 − 4.0N, indicating insufficient stress levels for martensitic transformation activation. Elevated temperature testing at 100°C revealed substantial property enhancement: loading stiffness increased to 307.7 − 382.3N/m (3-fold enhancement), energy dissipation reached 0.01 − 0.036J per cycle, and SEA achieved $5.7 - 20.0 \times 10^4 J/m^3$. The unloading path exhibited reduced stiffness of 334.4 − 478.3N/m, confirming hysteretic behavior characteristic of stress-induced phase transformation. These temperature-dependent mechanical property variations validate superelastic activation above the austenite finish temperature, establishing the critical role of thermal conditions in SMA component performance.

3.2. Assembly Performance and Scale-Up Validation

System-level assembly testing demonstrated substantial force enhancement compared to individual component performance, validating the parallel configuration design approach. Dual L-shaped sheet assemblies achieved average peak forces of 206.8 ± 24.9N at 5mm displacement during room temperature testing, representing approximately 13-fold enhancement relative to individual component capacity (16N). This force multiplication validates the effectiveness of the parallel bending mechanism in mobilizing multiple SMA elements simultaneously. Energy dissipation analysis revealed 0.303 ± 0.005J per cycle with SEA of $1.89 \pm 0.03 \times 10^5 J/m^3$, demonstrating efficient material utilization in the assembly configuration.

The assembly configuration demonstrated stable hysteretic behavior across multiple loading cycles, with consistent energy dissipation characteristics indicating reliable superelastic response. Force-displacement curves exhibited characteristic flag-shaped loops throughout testing, confirming maintained phase transformation behavior at the system level. Minimal residual deformation upon unloading validated effective self-centering capabilities inherent to the SMA material properties, with the parallel configuration preserving individual component superelastic characteristics while achieving substantial force capacity enhancement.

3.3. Configuration Performance Trade-Offs

Systematic comparison of the three device configurations under identical testing conditions revealed distinct performance trade-offs optimizing different structural parameters. Table 1 presents comprehensive performance metrics for all configurations tested at 5mm displacement and 25°C, enabling direct comparison under controlled conditions.

Table 1. Configuration performance comparison at 5mm displacement, 25°C

Configuration	Force (N)	Stiffness (N/mm)	SEA (J/m^3)	Recovery (%)
L-shape+Springs	224.5 ± 17.4	30.1 ± 0.7	$8.1 \pm 1.0 \times 10^4$	99.5
L-shape	206.8 ± 24.9	28.5 ± 1.4	$1.89 \pm 0.03 \times 10^5$	–**
Steel	183.7 ± 8.7	47.7 ± 2.8	Not comparable*	97.8

*Steel energy dissipation not compared due to plastic deformation effects
**Recovery ratio requires dynamic cyclic testing; static protocol insufficient

The combined sheet-spring configuration achieved maximum force capacity of 224.5N, representing optimal performance for high-load applications. However, this configuration exhibited reduced SEA (8.1×10^4J/m^3) compared to the individual L-shaped sheet configuration (1.89×10^5J/m^3), indicating trade-offs between force capacity and material efficiency. The sheet-spring assembly demonstrated superior self-centering capability with 99.5% recovery ratio, validating the enhanced restoring force concept.

Steel baseline testing confirmed conventional material limitations for seismic applications. While steel configurations achieved competitive stiffness (47.7N/mm) and good recovery ratio (97.8%) under static conditions, force-displacement curves exhibited permanent plastic deformation beyond yield stress. This plastic behavior prevents direct energy dissipation comparison with superelastic SMA configurations, as steel dissipates energy through irreversible deformation rather than reversible phase transformation. The steel baseline validates SMA advantages in maintaining structural integrity through cyclic loading.

Individual L-shaped Ni-Ti configurations demonstrated balanced performance across all metrics, achieving intermediate force capacity while maintaining highest SEA efficiency. This balanced characteristic positions individual sheet configurations as optimal for applications requiring simultaneous energy dissipation and structural capacity without geometric complexity.

3.4. Temperature Effects on SMA Performance

Temperature-dependent testing revealed substantial thermal effects on SMA device performance, establishing thermal control as a design parameter for performance optimization. Table 2 quantifies force enhancement across temperature conditions for L-shaped configurations.

Table 2. Temperature effects on L-shaped Ni-Ti assembly performance

Displacement	25°C Force (N)	100°C Force (N)	Enhancement (%)
±1.25mm	40.9 ± 4.1	77.3 ± 0.2	+88.9
±2.5mm	76.5 ± 1.5	169.3 ± 3.5	+121.4
±5mm	206.8 ± 24.9	405.9 ± 5.3	+96.3

Elevated temperature testing demonstrated substantial force enhancement across all displacement levels, with maximum enhancement of +121% observed at 2.5mm displacement. This temperature-dependent force increase results from enhanced austenitic phase stability at elevated temperatures, requiring higher stress levels to initiate martensitic transformation. The force enhancement enables adaptive performance tuning through thermal control strategies.

The experimental investigation establishes that no single configuration provides universal performance superiority across all metrics. Instead, each configuration optimizes distinct structural parameters, supporting a mission-specific design philosophy where device selection depends on prioritized seismic performance requirements. Steel configurations maintain relevance for applications prioritizing structural stiffness under static conditions, while SMA configurations demonstrate clear advantages in self-centering capability and cyclic loading resilience. The substantial temperature-dependent performance variations establish thermal control as a key enabling technology for adaptive SMA device optimization, with force enhancement capabilities exceeding 100% through controlled thermal management. These static characterization results provide essential foundation for subsequent dynamic validation studies under representative seismic loading conditions.

4. Conclusions

This investigation developed and characterized a novel L-shaped Ni-Ti seismic damping device through comprehensive quasi-static testing, establishing performance benchmarks across multiple configurations and thermal conditions. The experimental program successfully demonstrated systematic scale-up from individual components to functional assembly systems, achieving 13-fold force enhancement through parallel bending mechanisms.

Configuration comparison revealed distinct performance trade-offs rather than universal superiority. Combined sheet-spring assemblies optimize self-centering capability (99.5% recovery) with maximum force capacity (224.5N), while individual L-shaped configurations achieve highest efficiency ($1.9 \times 10^5 J/m^3$). Steel baseline testing confirmed conventional material limitations through irreversible plastic deformation, validating SMA advantages in maintaining structural integrity under cyclic loading.

Temperature effects demonstrated substantial performance tunability, with force enhancement exceeding +121% through thermal control from 25°C to 100°C. This thermal sensitivity establishes adaptive performance optimization opportunities through controlled thermal management strategies tailored to mission-specific requirements.

The static characterization provides essential foundation for subsequent dynamic validation. Future investigations will focus on shake table testing under representative seismic loading protocols, fatigue characterization through extended cycling, and thermal control system integration. The mission-specific design approach identified through this study enables optimized device selection based on prioritized structural performance requirements, advancing SMA-based seismic protection toward practical implementation.

References

Costanza, G., Mercuri, S., Porroni, I., Tata, M.E., 2024. Shape Memory Alloys for Self-Centering Seismic Applications: A Review on Recent Advancements. Machines 12, 628.

Mashal, M., Palermo, A., 2019. Low-damage seismic design for accelerated bridge construction. Journal of Bridge Engineering 24(7), 04019066.

Costanza, G., Porroni, I., Tata, M.E., 2024. Exploring the elastocaloric effect of Shape Memory Alloys for innovative biomedical devices: a review. Frattura ed Integrità Strutturale 18(70), 257–271.

Acar, E., 2015. Dynamic mechanical response of a Ni 45.7 Ti 29.3 Hf 20 Pd 5 alloy. Materials Science and Engineering A 633, 169–175.

DesRoches, R., McCormick, J., Delemont, M., 2004. Cyclic properties of superelastic shape memory alloy wires and bars. Journal of Structural Engineering 130(1), 38–46.

Miller, D.J., Fahnestock, L.A., Eatherton, M.R., 2012. Development and experimental validation of a nickel-titanium shape memory alloy self-centering buckling-restrained brace. Engineering Structures 40, 288–298.

Wang, B., Zhu, S.Y., 2018. Superelastic SMA U-shaped dampers with self-centering functions. Smart Materials and Structures 27(5), 055003.

Gao, N., Jeon, J.S., Hodgson, D.E., DesRoches, R., 2016. An innovative seismic bracing system based on a superelastic shape memory alloy ring. Smart Materials and Structures 25(5), 055030.

Qian, H., Li, H., Song, G., Guo, W., 2013. Recentering Shape Memory Alloy Passive Damper for Structural Vibration Control. Mathematical Problems in Engineering 2013, 1–13.

Qiu, C.X., Zhu, S.Y., 2017. Shake table test and numerical study of self-centering steel frame with SMA braces. Earthquake Engineering & Structural Dynamics 46(1), 117–137.

Chowdhury, M.A., Rahmzadeh, A., Alam, M.S., 2019. Improving the seismic performance of post-tensioned self-centering connections using SMA angles or end plates with SMA bolts. Smart Materials and Structures 28(7), 075044.

Wang, B., Zhu, S., Chen, K., Huang, J., 2020. Development of superelastic SMA angles as seismic-resistant self-centering devices. Engineering Structures 218, 110836.

Bizzarri, G., Costanza, G., Porroni, I., Tata, M.E., 2025. Mechanical Response and Elastocaloric Performance of Ni-Ti Shape Memory Alloy Sheets Under Varying Strain Rates. Compounds 5(2), 13.